Nanoscale

COMMUNICATION

View Article Online
View Journal | View Issue

Cite this: *Nanoscale*, 2015, **7**, 11531

Received 15th May 2015,
Accepted 3rd June 2015

DOI: 10.1039/c5nr03197d

www.rsc.org/nanoscale

A quinoxaline based N-heteroacene interfacial layer for efficient hole-injection in quantum dot light-emitting diodes†

Linyi Bai,‡[a] Xuyong Yang,‡[b] Chung Yen Ang,[a] Kim Truc Nguyen,[a] Tao Ding,[b] Purnandhu Bose,[a] Qiang Gao,[a] Amal Kumar Mandal,[a] Xiao Wei Sun,*[b] Hilmi Volkan Demir*[b] and Yanli Zhao*[a,c]

A series of N-heterocyclic quinoxaline derivatives was successfully synthesized and applied as hole transport layers in quantum dot light-emitting diodes (QLEDs). By inducing sp^2 N-atoms into the quinoxaline backbone, the electron affinity of the obtained material was enhanced, and its optical properties and bandgap became tunable. Quinoxaline based N-heteroacenes show a narrow bandgap, high thermal stability, and aligned film morphology. The resulting N-heteroacene polymer based QLED exhibits superior performance to poly(9-vinylcarbazole) based QLED. This study presents a strategy towards the design of novel N-rich molecules for the fabrication of QLEDs with improved performance.

Over the past few decades, molecules with extensive aromatic systems have been widely investigated and explored for their potential applications in organic optoelectronics,[1,2] which include organic light emitting diodes (OLEDs),[3,4] quantum dot light-emitting diodes (QLEDs),[5–8] organic field effect transistors (OFETs)[9–12] and photovoltaic cells.[13,14] Among the aromatic systems, special interest lies in acenes. As the leading charge transport materials in organic semiconductors, they have recently been extended to a family of N-heteroacenes. Such interest has arisen due to the promising development of novel high-performance organic semiconductors by introducing N atoms to the backbones in order to tune the electronic structure and molecular packing as well as increase the stability and solubility.[15,16] Recently, Houk *et al.*[17] designed a new strategy through the use of *N*-substituted acenes, which exhibited promising electron-transport behavior for their high electron affinities. Moreover, N-heteroacenes are believed to be less sensitive towards degradation through oxidation or dimerization.[18,19] In particular, the combinations of various numbers, positions and valence states of N atoms in N-heteroacenes could, in principle, yield a large number of structurally related π-backbones, which may bring considerable freedom to design organic semiconductors based on N-heteroacenes.[20,21] Thus, such studies would be very useful to build frameworks for describing the inherent influence and promoting our understanding on the associated structure–property relationships.

Whether N-heteroacenes are much superior to acenes or not depends on the performance of devices based on N-heteroacenes and acenes as the transport layers. Among the various devices, QLEDs have recently gained a lot of popularity due to their pure and saturated emission colors with a narrow bandwidth.[22–24] Currently, poly(9-vinylcarbazole) (PVK) is a widely used hole-transport interfacial layer for the fabrication of QLEDs. The highest efficiency values for all the blue, green and red emitting QLEDs are based on PVK as the hole-transport layer.[25–27] However, the performance of QLEDs in terms of brightness, efficiency and lifetime still needs to be further improved to meet the requirements of commercialization in the near future. Recently, scientists have explored various methodologies, including the development of highly efficient quantum dots with core–shell structures or with different compositions,[28,29] the modification of the surface of quantum dots,[30] and the changes in transport layers,[31,32] to match the energy level in order to promote the performance of the devices. In this work, we designed and synthesized a series of quinoxaline derivatives with π-conjugated N-heterocycles by condensation reactions between *ortho*-diaminoacenes and *ortho*-diketoacenes,[9] and explored their photophysical pro-

[a]*Division of Chemistry and Biological Chemistry, School of Physical and Mathematical Sciences, Nanyang Technological University, 21 Nanyang Link, Singapore 637371. E-mail: zhaoyanli@ntu.edu.sg*
[b]*LUMINOUS! Centre of Excellence for Semiconductor Lighting and Displays, School of Electrical and Electronic Engineering, Nanyang Technological University, 50 Nanyang Avenue, Singapore 639798. E-mail: exwsun@ntu.edu.sg, hvdemir@ntu.edu.sg*
[c]*School of Materials Science and Engineering, Nanyang Technological University, 50 Nanyang Avenue, Singapore 639798*
† Electronic supplementary information (ESI) available: Synthesis and characterization details. See DOI: 10.1039/c5nr03197d
‡ These authors contributed equally to this work.

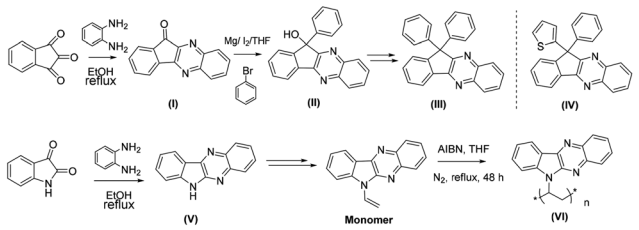

Scheme 1 Synthesis of N-heteroacene quinoxaline derivatives.

perties as well as their performance in QLEDs. Since these derivatives exhibit excellent thermal stability, optical properties, film morphology and hole transport capability, they can serve as efficient hole-transport materials.

The synthetic procedure of N-heteroacene quinoxaline derivatives is shown in Scheme 1. We mainly post-functionalized two N-heteroacene precursors. Precursor (**I**) is similar to fluorenone, which could be functionalized easily to afford compounds (**III**) and (**IV**). The other compound (**V**) containing N-heteroacene shows a close structural resemblance to carbazole. We then performed polymerization using the obtained monomer to prepare polymer PVI (**VI**), and studied its photophysical properties as compared with PVK due to their similar backbones.

In order to study optical properties, we measured the UV-Vis absorption and fluorescence spectra of these small molecules **II–IV** and polymer **VI**. It was observed from Fig. 1a that there were strong absorption peaks at ~280 nm and ~350 nm without an obvious difference among the three molecules **II–IV**. The corresponding emission of molecule **II** was at ~450 nm. There was an obvious shift in the emission wavelength upon the introduction of aromatic groups in compound **II** like benzene (**III**) and thiophene (**IV**). For polymer **VI**, we analyzed its adsorption and fluorescence properties in comparison with its monomer. It could be observed that the emission peak of the polymer shifted to 520 nm while the emission of the monomer was at 470 nm (Fig. 1b), indicating the enhancement in π-packing degree upon polymerization.

It is well known that the thermal stability and film morphology of semiconductor materials are very important in the device fabrication. Hence, we explored the thermal stability through the thermal-gravimetric analysis (TGA) by heating the samples from 10 °C min^{-1} to 1000 °C under a nitrogen atmosphere. The TGA results showed that the polymerization process enhanced the thermal stability of polymer **VI**, and the polymer only began to decompose at a temperature of 417.2 °C (Fig. 1c and S1 in ESI†). It could be observed that the resulting polymer had an obvious superiority in terms of thermal stability when compared with PVK. In addition, the polymer also exhibited good morphology upon film formation, which was probed by atom force microscopy (AFM, Fig. 1f and g). It could be seen that the film roughness is almost uniform and aligned. To further demonstrate the aligned film, powder X-ray diffraction (XRD) was performed (Fig. S2 in ESI†). Compared to the powder form of polymer **VI**, the powder XRD peaks for the thin film are sharper, and the ordered packing could be indicated by the similar distance among the sharp peaks. The thickness of the formed film could be controlled by tuning the spin-coating rate and the concentration of the sample solution

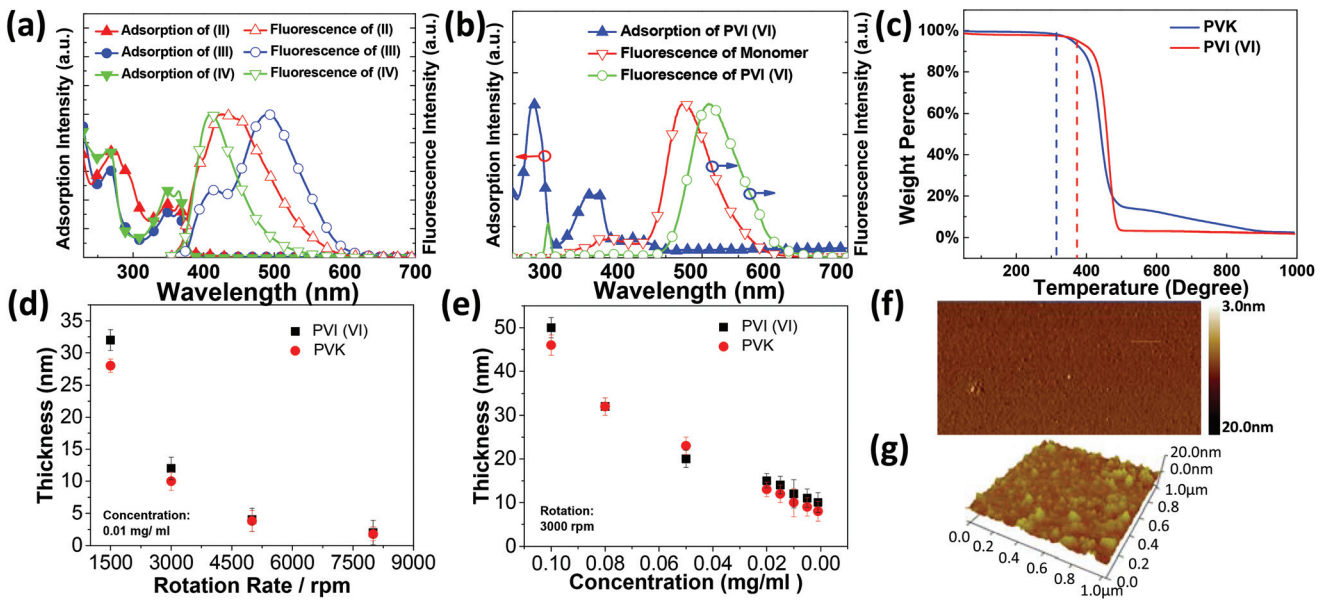

Fig. 1 Photophysical properties of quinoxaline derivatives and film morphology. (a,b) UV absorption and fluorescence spectra of small molecules (**II**, **III**, **IV**) and polymer (**VI**), respectively. The concentration of the sample solutions is 10^{-6} M in $CHCl_3$; (c) TGA curves of polymer PVI (**VI**) and PVK; (d,e) thickness of films obtained by using different rotation rates and concentrations. (f,g) AFM images of film morphology and a 3D diagram indicating the thickness and alignment.

Table 1 Energy level and bandgap of compounds and polymer

	Calculation		Experiment		
	HOMO	LUMO	HOMO[a]	LUMO[b]	Bandgap[c]
I	−6.90 eV	−3.18 eV	−6.77 eV	−3.24 eV	3.53 eV
Fluorenone	−6.73 eV	−3.01 eV	−6.64 eV	−2.87 eV	3.77 eV
V	−5.96 eV	−2.95 eV	−5.84 eV	−2.89 eV	2.95 eV
Carbazole	−5.83 eV	−2.27 eV	−5.76 eV	−2.14 eV	3.62 eV
VI	−5.94 eV	−2.90 eV	−6.02 eV	−2.97 eV	3.05 eV
PVK	−5.93 eV	−2.32 eV	−5.80 eV	−2.20 eV	3.60 eV

[a] Calculations for the HOMO based on the cyclic voltammogram by using the equation: $E_{HOMO} = (-4.8 + E_{ref} - E_{ox})$ eV, where $E_{ref} = (E_{ox} + E_{red})/2$, and E_{ox} and E_{red} refer to the oxidation and reduction potentials, respectively. [b] Values obtained from E_{HOMO} and the optical bandgap. [c] $E_g = 1240/\lambda_{max\text{-}edge}$, where $\lambda_{max\text{-}edge}$ is the wavelength in nanometers.

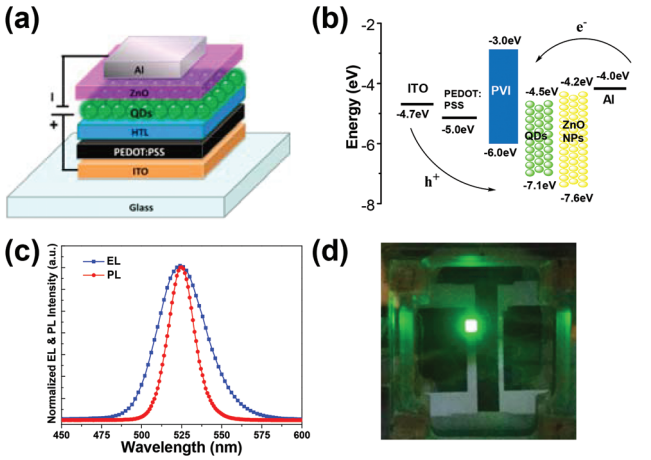

Fig. 2 (a) Schematic diagram of a layered polymer based QLED; (b) energy diagram of the device studied; (c) electroluminescence and photoluminescence spectrum of the device; (d) photographic image showing highly bright electroluminescence emission from the QLED using PVI (**VI**) as a HTL at an applied voltage of 5 V.

(Fig. 1d and e). Eventually, it was found that the film with 12 nm thickness was the most homogeneous one and had a high degree of alignment after annealing.

The electron density and bandgap could be affected significantly when N-atoms are introduced into the backbone of the arene systems. The density functional theory (DFT) calculation was performed to predict the bandgap of these materials using the Gaussian 09 W package for the optimization of the molecules through the basis set of B3LYP/6-311++G (d,p).[33] The optimization process also included adopting the polarization continuum model and using the integration formalism variant (IEFPCM) with chloroform as the solvent. The results showed that the lowest unoccupied molecular orbital (LUMO) of the molecules was reduced significantly after the nitrogen introduction, while no remarkable change occurred in the highest occupied molecular orbital (HOMO). Especially for the resulting polymer **VI**, the bandgap was 3.05 eV with the HOMO and LUMO energy levels at −5.94 eV and −2.90 eV, respectively (Table 1). The cyclic voltammetry (CV) measurements were also performed, showing the presence of a reversible reduction curve (Fig. S3 in the ESI†). In addition, the bandgap obtained from the CV measurements revealed a value of 2.97 eV for polymer **VI**, which is close to the theoretical result. On comparing with conventional compounds, the presence of the N atoms indeed induces a perturbation of the energy level, thus suggesting the possibility of tuning the energy level.

A semiconductor with a tunable bandgap could allow the material to adapt different operating conditions, thus widening its application scope. This is particularly the case for polymers consisting units with a tunable bandgap, such as PVI (**VI**). The aligned π-conjugated backbone of these acene units offers potential for carrier transport capability. Moreover, the presence of N atoms in the polymer promotes the electron affinity, allows the stability, solubility and molecular packing to be controlled, and thus enables the polymer to serve as a superior candidate for hole transport material. Based on these advantages, we studied the charge transport properties by using organic field-effect transistors (OFETs) with a top-contact and bottom-gated architecture (see the ESI† for the fabrication details). The devices were then thermally annealed at various temperatures for 10 min. The transfer curves of the OFET devices fabricated by PVI (**VI**) and PVK under as-cast conditions can be found in Fig. S7 (ESI†). Higher hole mobility and lower gate voltage (V_G) of OFET based on PVI (**VI**) further indicate that the presence of N atoms in the polymer backbone could efficiently improve the packing capability between the units, and decrease the HOMO level, facilitating the hole transport into the quantum dot (QD) layer to enhance the performance of the device.

Then, we proceeded to investigate the hole transport capability of PVI and PVK based QLEDs we fabricated, as shown in Fig. 2a. The structure of a conventional QD device consists of glass substrate/ITO/PEDOT:PSS/HTL (hole transport layer)/QDs/ZnO/Al, and the corresponding band diagram is shown in Fig. 2b. Core–shell CdSe/ZnS QDs were used as the emissive layer. A ZnO nanoparticle film serving as the electron transport layer (ETL) was spin-cast using ZnO nanoparticles in butanol solution. The electrons and holes are expected to recombine in a radiative fashion inside the QD layer so that efficient emission from the QDs can be produced. In our study, the performance of the device with PVI (**VI**) as the HTL was comparable to that of PVK. The electroluminescence (EL) spectrum of the fabricated QLEDs was recorded under an applied voltage of 5 V. The maximum emission band in the EL spectrum centered at λ = 524 nm with a full width at half-maximum of 34 nm, indicating highly efficient recombination of electrons and holes in the QD emissive layer (Fig. 2c). When compared with the corresponding photoluminescence (PL) spectrum of the QD solution, it can be noted that the EL spectrum of the resulting QLEDs is obviously broadened due to a combination of finite dot-to-dot interactions in close-packed solid films.[34] Fig. 2d displays a photograph of a PVI polymer-based QLED at an

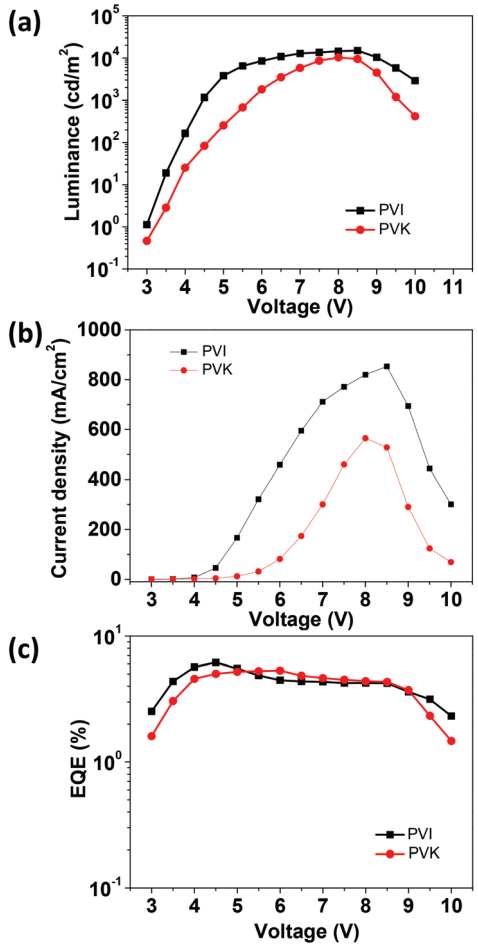

Fig. 3 (a) Luminance–voltage characteristics of the QLED devices with PVI (black line) and PVK (red line) as the HTL; (b) current density–voltage characteristics of the QLED devices with the same structures as (a); (c) external quantum efficiency *versus* voltage characteristics for the devices with PVI (black line) and PVK (red line) as the HTL.

applied voltage of 5 V, which exhibits uniform and bright green emission.

For the device performance, Fig. 3a and b show the current density–voltage and luminance–voltage characterization of conventional QLED devices using PVI and PVK as the HTL, respectively. Here, the turn-on voltage was defined when the luminance reached 1 cd m^{-2}. It was observed that the turn-on voltage was 3.0 V for the PVI based QLED, while it was 3.5 V for the PVK based QLED (Fig. 3a). In addition, the PVI-based QLED could reach the maximum voltage first and exhibit better stability upon increasing the applied voltage as compared with the PVK-based device. This observation indicates that using PVI as the HTL could allow the device to be turned on at a lower voltage so that it would be much safer and cost effective with lower energy consumption. Moreover, the resulting current density level of the QLED based on PVI as the HTL was ~850 mA cm^{-2}, which was higher than the PVK based QLED with ~560 mA cm^{-2} (Fig. 3b). This indicates that, under the same applied voltage, the radiative recombination of the electrically excited QDs in the PVI-based QLED was more efficient than that in the PVK-based QLED. Moreover, the external quantum efficiency (EQE) against the applied voltages for the devices (Fig. 3c) was also plotted. The QLED based on PVI as the HTL has a higher maximum EQE value of 6.24% compared with 5.26% provided by the QLED based on PVK as the HTL. The beneficial effect of the N-heterocyclic unit is appreciable in the PVI-based QLED as compared with the PVK-based QLED, since the additional N atoms could promote the electron affinity and molecular packing, enhance the hole transport capability, and ultimately improve the device efficiency. The density–voltage characteristics of the hole-only devices show that the PVI based device provides a higher current density under the same applied voltages (Fig. S8 in the ESI†), further indicating that PVI (**VI**) has a better hole transporting ability than PVK. In addition to the higher hole mobility, the HOMO level of PVI (**VI**) is closer to that of the ZnS QD shell when compared to that of PVK. As a result, the overcoming energy barrier in the hole injection is reduced so that more holes can be injected into the QDs, leading to enhanced exciton recombination in the QD layer.

In summary, we have successfully synthesized quinoxaline based N-heteroacene semiconductor materials. DFT calculations reveal that the electron density and bandgap could be influenced significantly when N atoms are introduced into the backbone of arenes. Particularly in PVI polymer **VI**, the introduction of N atoms effectively improves the packing between units and leads to a change in the energy level. This N introduction methodology makes the N-heteroacene materials match well with other functional layers on the energy level, so that the mobility and current density are further promoted when compared to PVK. The conclusion has been fully supported by the QLED characteristics and the space charge limited current (SCLC) measurements. Thus, PVI as the HTL in QLEDs contributes to improved current density, brightness, and maximum EQE value over PVK. We expect that this study will attract more interest towards the design of novel semiconductor molecules as well as the improvement of the existing organic electronic materials.

This research was supported by the National Research Foundation (NRF), Prime Minister's Office, Singapore under its NRF Fellowship (NRF2009NRF-RF001-015), Competitive Research Programme (NRF-CRP-6-2010-02 and NRF-CRP-11-2012-01), and Campus for Research Excellence and Technological Enterprise (CREATE) Programme – Singapore Peking University Research Centre for a Sustainable Low-Carbon Future. The research was also supported by the NTU-A*STAR Silicon Technologies Centre of Excellence under the program grant No. 11235100003.

Notes and references

1 S. S. Zade and M. Bendikov, *Angew. Chem., Int. Ed.*, 2010, **49**, 4012–4015.

2 J. E. Anthony, *Angew. Chem., Int. Ed.*, 2008, **47**, 452–483.
3 K. Brunner, A. van Dijken, H. Borner, J. Bastiaansen, N. M. M. Kiggen and B. M. W. Langeveld, *J. Am. Chem. Soc.*, 2004, **126**, 6035–6042.
4 A. van Dijken, J. Bastiaansen, N. M. M. Kiggen, B. M. W. Langeveld, C. Rothe, A. Monkman, I. Bach, P. Stossel and K. Brunner, *J. Am. Chem. Soc.*, 2004, **126**, 7718–7727.
5 V. Wood, M. J. Panzer, J. E. Halpert, J. M. Caruge, M. G. Bawendi and V. Bulovic, *ACS Nano*, 2009, **3**, 3581–3586.
6 J. M. Caruge, J. E. Halpert, V. Wood, V. Bulovic and M. G. Bawendi, *Nat. Photonics*, 2008, **2**, 247–250.
7 B. S. Mashford, M. Stevenson, Z. Popovic, C. Hamilton, Z. Zhou, C. Breen, J. Steckel, V. Bulovic, M. Bawendi, S. Coe-Sullivan and P. T. Kazlas, *Nat. Photonics*, 2013, **7**, 407–412.
8 Y. Shirasaki, G. J. Supran, M. G. Bawendi and V. Bulovic, *Nat. Photonics*, 2013, **7**, 13–23.
9 S. Allard, M. Forster, B. Souharce, H. Thiem and U. Scherf, *Angew. Chem., Int. Ed.*, 2008, **47**, 4070–4098.
10 C. A. Di, F. J. Zhang and D. B. Zhu, *Adv. Mater.*, 2013, **25**, 313–330.
11 M. M. Payne, S. R. Parkin and J. E. Anthony, *J. Am. Chem. Soc.*, 2005, **127**, 8028–8029.
12 F. J. Zhang, C. A. Di, N. Berdunov, Y. Y. Hu, Y. B. Hu, X. K. Gao, Q. Meng, H. Sirringhaus and D. B. Zhu, *Adv. Mater.*, 2013, **25**, 1401–1407.
13 N. Blouin, A. Michaud, D. Gendron, S. Wakim, E. Blair, R. Neagu-Plesu, M. Belletete, G. Durocher, Y. Tao and M. Leclerc, *J. Am. Chem. Soc.*, 2008, **130**, 732–742.
14 N. Blouin, A. Michaud and M. Leclerc, *Adv. Mater.*, 2007, **19**, 2295–2300.
15 Z. X. Liang, Q. Tang, J. B. Xu and Q. A. Miao, *Adv. Mater.*, 2011, **23**, 1535–1539.
16 Q. Tang, D. Q. Zhang, S. L. Wang, N. Ke, J. B. Xu, J. C. Yu and Q. Miao, *Chem. Mater.*, 2009, **21**, 1400–1405.
17 M. Winkler and K. N. Houk, *J. Am. Chem. Soc.*, 2007, **129**, 1805–1815.
18 B. D. Lindner, J. U. Engelhart, O. Tverskoy, A. L. Appleton, F. Rominger, A. Peters, H. J. Himmel and U. H. F. Bunz, *Angew. Chem., Int. Ed.*, 2011, **50**, 8588–8591.
19 A. L. Appleton, S. M. Brombosz, S. Barlow, J. S. Sears, J. L. Bredas, S. R. Marder and U. H. F. Bunz, *Nat. Commun.*, 2010, **1**, 94–100.
20 P. Y. Gu, F. Zhou, J. K. Gao, G. Li, C. Y. Wang, Q. F. Xu, Q. C. Zhang and J. M. Lu, *J. Am. Chem. Soc.*, 2013, **135**, 14086–14089.
21 G. Li, Y. C. Wu, J. K. Gao, C. Y. Wang, J. B. Li, H. C. Zhang, Y. Zhao, Y. L. Zhao and Q. C. Zhang, *J. Am. Chem. Soc.*, 2012, **134**, 20298–20301.
22 M. Zorn, W. K. Bae, J. Kwak, H. Lee, C. Lee, R. Zentel and K. Char, *ACS Nano*, 2009, **3**, 1063–1068.
23 K.-S. Cho, E. K. Lee, W.-J. Joo, E. Jang, T.-H. Kim, S. J. Lee, S.-J. Kwon, J. Y. Han, B.-K. Kim, B. L. Choi and J. M. Kim, *Nat. Photonics*, 2009, **3**, 341–345.
24 L. Qian, Y. Zheng, J. Xue and P. H. Holloway, *Nat. Photonics*, 2011, **5**, 543–548.
25 X. Dai, Z. Zhang, Y. Jin, Y. Niu, H. Cao, X. Liang, L. Chen, J. Wang and X. Peng, *Nature*, 2014, **515**, 96–99.
26 K.-H. Lee, J.-H. Lee, H.-D. Kang, B. Park, Y. Kwon, H. Ko, C. Lee, J. Lee and H. Yang, *ACS Nano*, 2014, **8**, 4893–4901.
27 K.-H. Lee, J.-H. Lee, W.-S. Song, H. Ko, C. Lee, J.-H. Lee and H. Yang, *ACS Nano*, 2013, **7**, 7295–7302.
28 W. K. Bae, J. Kwak, J. W. Park, K. Char, C. Lee and S. Lee, *Adv. Mater.*, 2009, **21**, 1690–1694.
29 E. Jang, S. Jun, H. Jang, J. Llim, B. Kim and Y. Kim, *Adv. Mater.*, 2010, **22**, 3076–3080.
30 X. Yang, D. Zhao, K. S. Leck, S. T. Tan, Y. X. Tang, J. Zhao, H. V. Demir and X. W. Sun, *Adv. Mater.*, 2012, **24**, 4180–4185.
31 W. K. Bae, J. Kwak, J. Lim, D. Lee, M. K. Nam, K. Char, C. Lee and S. Lee, *Nano Lett.*, 2010, **10**, 2368–2373.
32 J. Kwak, W. K. Bae, D. Lee, I. Park, J. Lim, M. Park, H. Cho, H. Woo, D. Y. Yoon, K. Char, S. Lee and C. Lee, *Nano Lett.*, 2012, **12**, 2362–2366.
33 M. J. T. Frisch, G. W. Trucks, H. B. Schlegel, G. E. Scuseria, M. A. Robb, J. R. Cheeseman, G. Scalmani, V. Barone, B. Mennucci and G. A. Petersson, *et al.*, *GAUSSIAN 09 (Revision A.2)*, Gaussian, Inc., Wallingford CT, 2009.
34 X. Yang, E. Mutlugun, C. Dang, K. Dev, Y. Gao, S. T. Tan, X. W. Sun and H. V. Demir, *ACS Nano*, 2014, **8**, 8224–8231.